



Quasiparticle poisoning in trivial and topological Josephson junctions

Aleksandr E. Svetogorov , Daniel Loss, and Jelena Klinovaja 

Department of Physics, University of Basel, Klingelbergstrasse, 4056 Basel, Switzerland



(Received 10 December 2021; revised 6 May 2022; accepted 19 May 2022; published 27 May 2022)

We theoretically study a short single-channel Josephson junction between superconductors in the trivial and topological phases. The junction is assumed to be biased by a small current and subjected to quasiparticle poisoning. We find that the presence of quasiparticles leads to a voltage signal from the Josephson junction that can be observed both in the trivial and topological phases. Quite remarkably, these voltage signatures are sufficiently different in the two phases such that they can serve as means to clearly distinguish between trivial Andreev and topological Majorana bound states in the system. Moreover, these voltage signatures, in the trivial and topological phases, would allow one to directly measure the quasiparticle poisoning rates and test various approaches for protection against quasiparticle poisoning.

DOI: [10.1103/PhysRevB.105.174519](https://doi.org/10.1103/PhysRevB.105.174519)

I. INTRODUCTION

Majorana fermions in condensed matter physics have been a hot topic in the community ever since the first claim that these non-Abelian anyons can exist in mesoscopic systems [1]. Nevertheless, experimental realization of a system supporting Majorana bound states (MBSs) as well as direct observation of these bound states presents a sophisticated problem. Despite numerous claims of indirect observation of MBSs, there have always been concerns that the demonstrated effects may have different origins. One of the biggest problems is quasiparticle poisoning (QP), which causes a change of the fermion parity, while the Majorana qubit is based on a fixed-parity model, as well as the majority of effects proposed to establish the presence of MBSs in a system, such as fractional Josephson effect [1–4]. Despite being studied over the last decade [5–11], QP still requires both theoretical and experimental attention, as different theoretical approaches lead to different estimates on the QP rates mostly due to accounting for different sources of quasiparticles. In this paper, we propose that the high sensitivity of devices with MBSs can actually be used to indicate the topological phase as well as to measure the QP rates and to get a better understanding of the possible mechanisms leading to QP. Moreover, we discuss the effect of poisoning in case of trivial (single-channel) Josephson junctions (JJs) and show that it is principally different from the effect in the topological phase, which provides an unambiguous way to distinguish Andreev bound states (ABSs) in the trivial phase from MBSs in the topological phase.

In this paper, we focus on a short single-channel JJ that can host MBSs in the topological phase. Different physical realizations for such JJs have been proposed [3,12–16]. Here we will assume a JJ based on a nanowire with Rashba spin-orbit interaction (SOI) in a magnetic field B parallel to the wire, resulting in the Zeeman energy $V_Z = \frac{1}{2}g\mu_B B$ (g is Landé g factor, μ_B is Bohr magneton). An s -wave superconductor induces a proximity gap Δ in the nanowire, which makes the nanowire an effective one-dimensional superconductor. One should note that this Δ in general is decreasing with the field

V_Z (and very strong fields destroy superconductivity). While we focus on explicit calculations on nanowires, our results are more general and also apply to other JJ platforms such as topological insulators [12,15,17] and quantum spin Hall edge systems [3]. A junction is formed in an area of nanowire not covered by the superconductor. The system is driven in the topological phase if the Zeeman field is above the critical value: In a simplified model with the Fermi level in the middle of the Zeeman gap, the transition occurs at $V_Z = \Delta$ [18]. In the topological phase, a pair of MBSs, localized on the junction sides, creates an effective channel for single-quasiparticle tunneling, see Fig. 1. As a result, this tunneling is usually expected to be characterized by the energy scale $E_M \sim \sqrt{D_N \Delta_c}$ [3,19], corresponding to the overlap of the MBSs on the JJ, D_N is the normal state transmission of the JJ and Δ_c is the topological bulk gap. As long as we can neglect the overlap with another pair of MBSs, localized on the outer sides of the topological part of the system, the only mechanism to change the parity of the state formed by MBSs on the JJ is to absorb a quasiparticle. The parity switching events occur on timescales much shorter than any other process in the system, which allows us to work in a fixed-parity regime in between such switching events. The process is usually treated by a Fokker-Planck equation [20,21]; we can consider the parity switch to be a random event with characteristic timescale τ_{qp} between two events. Between the switching events, we can use the fixed-parity model. Topological JJs differ from anontopological JJs by a 4π -periodic term in the Hamiltonian, corresponding to single-electron tunneling [3,19]. If the junction is biased by an electrical current I , the Hamiltonian of the system takes the form (we put $\hbar = 1$ throughout)

$$H = \frac{q^2}{2C} + U(\phi), \quad (1)$$

$$U(\phi) = -U_{2\pi}(\phi) - U_{4\pi}(\phi) - I\phi/(2e), \quad (2)$$

where $U(\phi)$ is the effective phase potential, consisting of $U_{2\pi}(\phi)$ and $U_{4\pi}(\phi)$ corresponding to a Cooper pair and a single electron (due to MBSs) tunneling, respectively, and bias

current contribution (last term); C is the capacity of the JJ, q is the charge accumulated on the junction, e is the absolute value of the electron charge. The sign of the 4π -periodic term is determined by the fermionic parity [3,22]. In this paper, we focus on a specific case: We consider the regime of well-defined phase ϕ , which requires tunneling terms to dominate over Coulomb interactions, i.e., $E_J + E_M \gg E_c = \frac{e^2}{2C}$. Another assumption is that the junction is short (with the length $l \ll \xi$, where ξ is the superconducting coherence length) with relatively small cross section $S \ll \xi^2$. The Hamiltonian H defined in Eq. (1) corresponds to an ideal system without dissipation. To include dissipation into consideration, we use the resistively shunted junction (RSJ) model [23,24], which allows us to treat the junction as an ideal junction shunted by a resistance R , which is defined by quasiparticle current and depends explicitly on the experimental setup. We assume an overdamped JJ regime $R \ll R_Q$ as experimentally relevant, where $R_Q = 2\pi/(2e)^2$ is the resistance quantum.

The phase potential, in general, can be defined as a ground-state energy with the fixed parity and phase ϕ of the many-body Hamiltonian in its eigenbasis [25],

$$H(\phi) = \sum_b E_b(\phi) \left(n_b - \frac{1}{2} \right) + \sum_i E_i(\phi) \left(n_i - \frac{1}{2} \right) + H_0, \quad (3)$$

where $E_b(\phi)$ are the bound-state energies—either the ABSs in the trivial phase, or the bound state formed by two MBSs in the topological phase— n_b is the occupation of each state, $|\Delta - V_Z| < E_i(\phi) < \Delta$ are the energies of the continuum states, n_i is the number operator for fermions in each continuum state, and H_0 is the phase-independent contribution. In a trivial JJ, $U_{2\pi}(\phi)$ is determined by the sum of the ABSs' energies, which are formed in the JJ, and continuum contribution (which is absent without magnetic field); in a topological JJ, $U_{4\pi}(\phi)$ is given by a single bound-state energy (which is 4π periodic) and again the 2π -periodic continuum contribution. The simple cosine phase dependencies of the bound-state energies are not general but valid for a JJ with low normal-state transparency. Nevertheless, the phase periodicity is general: 2π periodicity for the trivial and 4π periodicity for the topological phase. As long as the occupation of the bound states is unchanged, one can treat the sum of these terms as the phase potential. Whenever the occupation of one bound states changes, the phase dependencies in the phase potential change, too, which may have a significant effect on the phase evolution.

II. PARITY SWITCHING

Quasiparticles are created through Cooper pair breaking in the superconductor. The effect is crucial for the stability of topological qubits formed by MBSs; several approaches to estimate it were proposed [5–11,26], however, universal and experimentally verified estimates still do not exist. It was shown that, upon creation, quasiparticles rapidly relax to the continuum edge, while the further process of recombination into Cooper pairs or trapping into subgap states is relatively slower [27,28]. For temperatures sufficiently lower than the superconducting critical temperature, the creation of

quasiparticles due to thermal fluctuations [29] is exponentially suppressed and can be neglected. However, several experiments have reported quasiparticle density saturation at low temperatures [27,30–32], which indicates other sources for quasiparticle creation. The observed densities of quasiparticles allow one to estimate the QP rates in various systems; for semiconducting nanowires proximitized by a bulk superconductor the estimation shows high decoherence rates [7]: $\Gamma_{\text{qp}} \gtrsim 1 - 10$ MHz. It was shown experimentally that QP in different superconducting qubits may soon get the dominant source of contribution for decoherence, as the techniques to reduce decoherence from other sources are being developed [33–36]. In combination with experimental evidence [34,37], it seems that the main source of quasiparticles at low temperatures is radioactivity, specifically radioactive muons and/or gamma rays. The mechanism of quasiparticle bursts created by muons was theoretically described in Ref. [38], later optimistic estimations have been made [11], assuming that for small enough devices ($V = 10\mu\text{m} \times 200\text{nm} \times 10\text{nm} = 2 \times 10^{-2}\mu\text{m}^3$) the effect can be neglected ($\Gamma_{\text{qp}}^{-1} \sim 10$ days); however, the estimates rather contradict the experimentally observed values of QP rates [27,39] for similar-size superconducting devices. It is plausible that the main reason for this discrepancy is that the entire setup, including substrate and connections, contributes to the muon absorption, while the resulting phonons can easily propagate from anywhere to the superconducting part of the setup where they create quasiparticle excitations [34,35]. However, this suggestion requires further investigation, especially on the specific samples which are expected to host MBSs.

III. VOLTAGE DUE TO QP IN THE TRIVIAL PHASE

In the trivial phase, nonequilibrium quasiparticles can recombine pairwise or relax into a subgap ABS. The latter effect is usually not easy to observe in a typical SNS-JJ with $n \gg 1$ channels. If a quasiparticle gets trapped in one of the ABSs, the resulting change of the total Josephson energy is only of the order $E_J/n \ll E_J$, even though state-of-the-art experimental techniques allow one to observe E_J fluctuations [40]. However, in a single-channel JJ, which is the system studied in this paper, this argument is invalid ($n = 1$). We provide a detailed analysis of the subgap spectrum in the limit of strong SOI and low transparency in Appendix A (for high-transparency limit, see Refs. [25,41]). For small bias current, $I \ll I_c = 2eE_J$, the minima of the phase potential are slightly shifted from the value corresponding to $I = 0$: $\phi_{\text{min}} \approx 2\pi k + \frac{I}{2eE_J}$ with integer k , which results in a small energy gap between the continuum edge Δ_c (in the strong SOI limit $\Delta_c = \min[|\Delta - V_Z|, \Delta]$) and the bound state given by $\epsilon \approx I^2/(4e^2E_J) \ll \Delta_c$ at ϕ_{min} , see Fig. 2. At zero magnetic field, when the ABSs are degenerate, if a quasiparticle is trapped in one ABS, the only conducting channel will get poisoned, which would result in a running (resistive) state with voltage $V = IR$. Subsequently, the system relaxes back to the localized state due to recombination of the trapped quasiparticle with a quasiparticle from the continuum on a timescale $\tau_r \ll \tau_{\text{qp}}^{\text{triv}}$ (see discussion in Appendix A and Fig. 3). Upon introducing a magnetic field, the ABSs split as well as the bulk gap Δ_c getting smaller; the lower-energy ABS touches

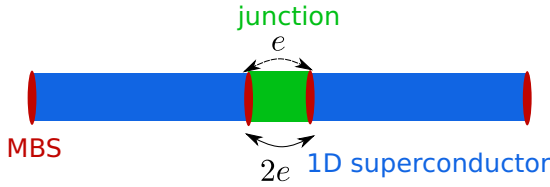


FIG. 1. A schematic representation of a topological JJ; $2e$ tunneling between one-dimensional superconductors corresponds to a trivial Cooper-pair tunneling, while MBSs (marked with red) allow for a single-electron (e) tunneling through the junction.

the continuum edge Δ_c at $\phi = 0$ and $\phi = 2\pi$, while the upper ABS partially merges with the continuum, see Fig. 2. The amplitude of the lower ABS is getting smaller than the higher ABS amplitude and the voltage in the running state is decreasing (quadratically in small Zeeman energy V_Z ; moreover, it is slowly varying in time) until no voltage is possible even with one quasiparticle trapped in the lowest ABS, as local minima of the phase potential get restored, see Fig. 2 and

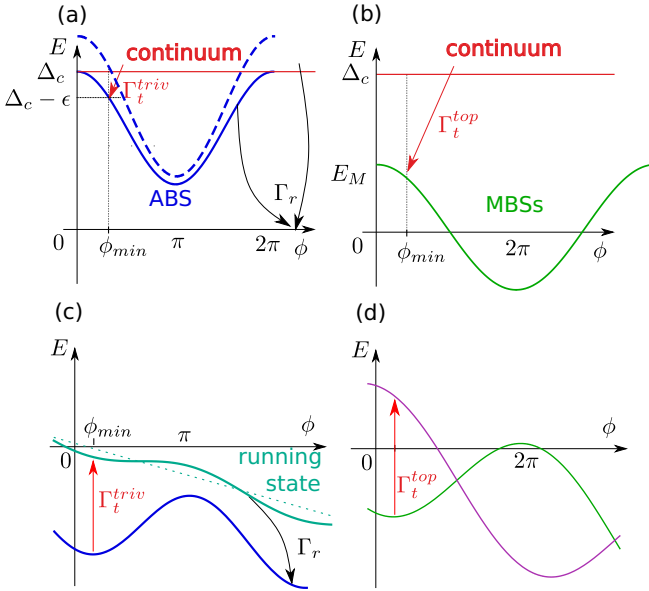


FIG. 2. A schematic of the single-particle spectrum of the JJ in (a) trivial and (b) topological phases. The red solid line represents the continuum edge Δ_c . Above-gap quasiparticles can get trapped in the bound states with the rate Γ_t^{triv} in the trivial and Γ_t^{top} in the topological phases. When one quasiparticle is trapped in the lower ABS [solid blue curve in (a); dashed blue curve represents the higher ABS partially merged with the continuum], it can recombine with a quasiparticle from the continuum with probability $\Gamma_r \gg \Gamma_t^{\text{triv}}$. The second row corresponds to the many-particle spectrum, given by Eq. (3), in (c) trivial and (d) topological phases with a linear shift $-I\phi/(2e)$ due to bias current. In the trivial phase (c), trapping a quasiparticle in an ABS excites the system from the ground state (blue curve) to a state represented by the green line, which has no local minima for low fields [for $V_Z = 0$ it is exactly linear, which is represented by the green dotted line in (c)], which results in the resistive (running) state. In the topological phase (d), there is only one bound state for each parity, therefore, excitation due to QP results in a state with the same amplitude in phase but with shifted local minima (green curve for even state, violet for odd).

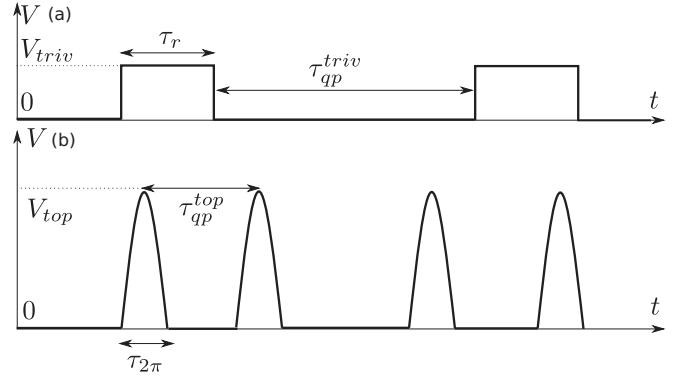


FIG. 3. A schematic of voltage pulses on the JJ (a) at low magnetic fields (trivial phase) and (b) in the topological phase. The upper panel (a) shows voltage pulses of size V_{triv} , given by Eq. (4), and length $\tau_r = \Gamma_r^{-1}$ and separated by $\tau_{\text{qp}}^{\text{triv}} \ll \tau_r$. These pulses correspond to the running (excited) state. In the lower panel (b), sharp voltage pulses of length $\tau_{2\pi} \ll \tau_{\text{qp}}^{\text{top}}$ and amplitude V_{top} estimated by Eq. (6) correspond to phase readjustment to the shifted phase potential after the parity switch. These voltage peaks are separated by $\tau_{\text{qp}}^{\text{top}} \ll \tau_{\text{qp}}^{\text{triv}}$.

discussion in Appendix A. As a result, we expect that it should be possible to experimentally observe voltage pulses of length τ_r and average amplitude (see Appendix C),

$$V_{\text{triv}} \approx R\sqrt{I^2 - e^2V_Z^2D_N^2}/16, \quad (4)$$

separated by $\tau_{\text{qp}}^{\text{triv}} \gg \tau_r$ for low fields and no voltage upon approaching the topological phase transition.

IV. VOLTAGE DUE TO QP IN THE TOPOLOGICAL PHASE

As shown for a short JJ based on a quantum spin Hall insulator [20,21], deep inside the topological phase, the phase potential is 4π -periodic (for zero bias current) due to a fermionic state formed by two MBSs localized on the sides of the JJ, which is equivalent to $U_{2\pi} = 0$ and $U_{4\pi} = (E_M/2)\cos(\phi/2)$ in Eq. (1). If the parity of this state is changed, the corresponding term in the many-body Hamiltonian changes signs, which effectively flips the phase potential. Therefore, if the system is in the ground state (localized in one of the minima of the phase potential), each parity switching event should result in a time evolution of this state, in the case of sufficient dissipation it will be relaxation to the nearby new minimum. The bias current I tilts the phase potential and, therefore, introduces asymmetry in the phase evolution. Then, as mentioned in Ref. [21], each parity switching event would result in a voltage pulse, as the phase slides by 2π to a new local minimum. The effect should be general for any JJ which can undergo a topological phase transition by varying some parameter (e.g., magnetic field). The situation is somewhat different close to the topological phase transition: in the topological phase, the phase potential is 4π periodic but has a significant 2π -periodic component due to the contribution from the continuum states [25,41,42], which creates additional odd local minima at $\phi = 2\pi(2k + 1)$, where k is integer. The change of the bound-state parity would only change the sign of the 4π -periodic component, therefore,

shifting even minima up and odd minima down in energy; the state would remain localized in the same local minimum of the phase potential. Nevertheless, deep inside the topological phase the 2π -periodic component is suppressed ($E_M \gg E_J$) and voltage pulses would be triggered by each parity switch if the JJ is biased by a small current.

We illustrate this general discussion with an effective model given by Hamiltonian H defined in Eq. (1) with cosine phase dependencies. The critical current $I_c = 2e(E_J + E_M/4)$ is determined as the maximum current at which the phase potential Eq. (2) has local minima. If we consider the low-temperature limit with no quasiparticles, the JJ is in the perfectly superconducting state and the wave function is trapped in a local minimum of the tilted washboard potential, as long as thermal fluctuations can be neglected, i.e., $T \ll E_M$. What we are interested in is the trapping of nonequilibrium above-gap quasiparticles into the bound states on the JJ. Deep inside the topological phase ($E_M \gg E_J$), the bound-state energy alone is given by $E = E_M \cos(\phi/2)$. In the regime of strong SOI and in the low-transparency limit (high-transparency limit was studied in Ref. [25]), we show that its amplitude scales linearly with D_N (see Appendix A):

$$E_M \approx 2 \frac{D_N \Delta}{V_Z} (V_Z - \Delta). \quad (5)$$

This state is separated from the continuum at any phase ϕ , which makes it prone to trap quasiparticles. Each parity switching event effectively shifts the local minima of the phase potential by 2π , causing the state to relax to this new minimum and, therefore, resulting in a voltage pulse

$$V_{\text{top}} \approx \frac{1}{2e} \frac{2\pi}{\tau_{2\pi}}, \quad (6)$$

where $\tau_{2\pi} \approx (\pi E_M R / R_Q)^{-1}$ [4,20,43] is the characteristic time for relaxation in a new 2π -shifted minimum calculated in the classical limit for an overdamped junction, see Fig. 3. The asymmetry of the phase evolution after the parity switch is determined by the bias current I . Then, the average voltage (averaged over many poisoning events) is given by a simple expression [21], which does not depend on the bias current as long as it is small,

$$\langle V \rangle = \frac{1}{2e} \frac{2\pi}{\tau_{\text{qp}}^{\text{top}}}, \quad (7)$$

where $\tau_{\text{qp}}^{\text{top}}$ is significantly shorter than $\tau_{\text{qp}}^{\text{triv}}$ in the trivial phase (see Appendix C),

$$\frac{\tau_{\text{qp}}^{\text{top}}}{\tau_{\text{qp}}^{\text{triv}}} \approx \frac{I^4}{(2e)^4 E_J^2 (\Delta_c - E_M)^2} \ll 1, \quad (8)$$

as the bound state is well separated from the continuum $\Delta_c - E_M \gg I/(2e)$. Equation (7) is valid as long as $\tau_{\text{qp}}^{\text{top}} < \tau_{2\pi}$, otherwise the phase does not readjust to the new minimum between the QP events; usually the phase relaxation is expected to be fast enough [21,43]. What is important is that we do not require a topological protection of the MBSs, more precisely, there is no need for exponential suppression of the MBSs overlap with the nanowire length, which might be hard (or even impossible) to realize due to phonons at any finite (phonon) temperature [44]. If the resulting anticrossing

[45,46] is sufficiently strong, the phase would slide only by π to the new minimum at the anticrossing and the resulting average voltage is reduced by a factor of 2 (see discussion in Appendix B).

V. MEASUREMENT

An important question is whether the discussed effect can be measured in a realistic experimental setup. First, there could be problems with measuring the average voltage in the topological phase due to QP, since in an ideal case one can distinguish a voltage of the order of hundred nanovolts, which requires the average time between the poisoning events to be of the order of ten nanoseconds or less to see the voltage given by Eq. (7). On the other hand, it seems that state-of-the-art experimental techniques should allow one to distinguish separate voltage peaks; using the estimate provided in Ref. [21] $\tau_{2\pi} \sim 10$ ps, which corresponds to a sharp peak of hundred μeV height (which is significantly higher than a typical noise signal), one can expect the measurement itself to last longer, however, measurements at frequency $\nu_m \sim 1$ GHz are feasible, which would result in a value of the order of $V_m \approx 2\pi\nu_m/(2e) \sim 1 \mu\text{V}$ measured for the phase shift of 2π expected after the parity switch. The voltage pulses in the topological phase are independent of the bias current in contrast to the ones in the trivial phase. Moreover, the voltage appears in the trivial phase only for low magnetic fields (parametrically low in I/I_c), while close to the phase transition there is no voltage signal due to QP. Finally, we show that the characteristic time between QP events in the topological phase is much shorter than in the trivial phase $\tau_{\text{qp}}^{\text{top}} \ll \tau_{\text{qp}}^{\text{triv}}$. For a voltage peak in the topological phase the integral of voltage over time (per peak) is a constant: $\int V_{\text{top}} dt = \pi/e$, while in the trivial phase voltage oscillates around some average value (or is constant for zero field), while the junction stays in the excited state. As a result, voltage pulses in the topological phase are much more frequent, with much larger amplitude but very short in time. The picture can differ in the case of significantly modified subgap spectrum, i.e., in the case of a quantum dot-based junction, when ABSs can be detached from the continuum, which would increase poisoning rates in the trivial phase. However, we expect that in typical single-channel junctions without additional gating, the subgap spectrum is qualitatively similar to the toy model we considered in this paper: in the trivial phase bound states touch the continuum edge or even merge with it, which makes QP probability rather low (and dependent on the small bias current) in comparison to the topological phase when the bound state is detached from the continuum edge. In general, we suggest that the experiment should be performed in the whole range of magnetic field, which should allow one to observe the rare current-dependent voltage signals in the trivial phase at low magnetic field, no signal in the large vicinity of the phase transition and, finally, sharp current-independent voltage peaks deep in the topological phase, if it can be realized in the experimental setup.

VI. CONCLUSIONS

In summary, we have proposed a set of experiments to observe the effects of QP in trivial and topological JJs.

Successful observation of sharp current-independent voltage pulses in the topological phase would be a reliable way to distinguish MBSs from ABSs. Moreover, measurements in both trivial and topological phases would allow one to estimate the rates of QP in each phase. The measurement in the trivial phase could be performed right away on existing single-channel junctions. Furthermore, performing experiments in different setups could be a way to test different sources of QP and develop efficient methods of protection against QP.

ACKNOWLEDGEMENTS

We want to thank V. Kurilovich, D. Lvov, and D. Antonenko for fruitful discussions. This paper was supported by the Swiss National Science Foundation and NCCR QSIT. This project received funding from the European Union's Horizon 2020 research and innovation program (ERC Starting Grant, Grant Agreement No. 757725).

APPENDIX A: THE LOW-ENERGY SPECTRUM OF A JOSEPHSON JUNCTION BASED ON A PROXIMITIZED SEMICONDUCTING NANOWIRE WITH STRONG SOI CLOSE TO THE PHASE TRANSITION

In this Appendix, we provide a detailed analysis of the low-energy spectrum of a topological JJ. We analyze the scaling of the phase potential amplitude (E_J for trivial phase and E_M for topological) with the normal state transmission amplitude D_N to validate our analysis of phase evolution after the parity switch in the main text. Our starting point is a linearization procedure [18] with subsequent calculation of the low-energy spectrum [25,41] for a JJ based on a semiconducting nanowire with strong Rashba SOI of strength α , as in this regime the junction is in the Andreev limit ($\Delta \ll E_F \sim m\alpha^2$, where E_F is the Fermi energy measured from the bottom of the conduction band and is set by the characteristic energy of SOI $\sim m\alpha^2$, where m is the effective electron band mass, Δ is the proximity gap). Another ingredient is the Zeeman field $V_Z = \frac{1}{2}g\mu_B B$ (g is Landé g factor, μ_B is Bohr magneton); one should note that the Andreev limit also requires V_Z to be small in comparison to SOI energy, i.e., $V_Z \ll m\alpha^2$. An additional assumption we make to simplify the analysis is that the Fermi level is exactly in the middle of the Zeeman gap. Let us briefly reproduce the main steps following the approach of Refs. [25,47]. The mean-field many-body Hamiltonian of the system is [13,22]

$$\hat{H} = \frac{1}{2} \int dx \hat{\Psi}^\dagger(x) \mathcal{H} \hat{\Psi}(x), \quad (\text{A1})$$

where $\hat{\Psi}^T = (\hat{\psi}_\uparrow, \hat{\psi}_\downarrow, \hat{\psi}_\downarrow^\dagger, -\hat{\psi}_\uparrow^\dagger)$ with $\hat{\psi}_\downarrow$ and $\hat{\psi}_\uparrow$ being annihilation operators of an electron with spin down and up, respectively. The Bogoliubov-de Gennes Hamiltonian is given by

$$\mathcal{H} = \left(-\frac{\partial_x^2}{2m} - i\alpha \partial_x \sigma_z - \mu + V(x) \right) \tau_z - V_Z \sigma_x + \Delta(x) \tau_x, \quad (\text{A2})$$

where τ_ν are the corresponding Nambu space Pauli matrices, μ the chemical potential measured from the middle of the

Zeeman gap at $k = 0$, m is the effective electron mass and σ_ν are the Pauli matrices acting in spin space. For simplicity, we proceed with $\mu = 0$, corresponding to the optimal point to enter the topological phase as it corresponds to the lowest phase transition field $V_z^c = \Delta$. Next we perform a procedure of linearization of the spectrum around the Fermi points [18]: $k = 0$ for inner modes and $k = \pm 2m\alpha = \pm 2k_{so}$ for the outer modes (here we have introduced the SOI momentum $k_{so} = m\alpha$). As a result, electron fields $\hat{\Psi}$ can be presented in terms of slowly varying right $\hat{\Psi}_R(x)$ and left $\hat{\Psi}_L(x)$ movers:

$$\hat{\Psi}(x) = \hat{\Psi}_R(x) e^{ik_{so}x(1-\sigma_z)} + \hat{\Psi}_L(x) e^{-ik_{so}x(1+\sigma_z)}. \quad (\text{A3})$$

If we use this decomposition and average out all fast oscillating terms $\sim \exp(-2k_{so}x)$, we get

$$(-i\alpha \sigma_x \tau_z - V_z \sigma_x + \Delta(x) \tau_x) \Psi_i(x) = E \Psi_i(x) \quad (\text{A4})$$

for the inner mode wave function and

$$(i\alpha \sigma_x \tau_z + \Delta(x) \tau_x) \Psi_o(x) = E \Psi_o(x) \quad (\text{A5})$$

for the outer mode wave function. The provided equations work in the whole structure except for the short junction region itself. To solve the equations, one needs to supplement them with suitable boundary condition at the short junction $x = 0$,

$$\Psi(0^+) = T \Psi(0^-), \quad (\text{A6})$$

where T is the transfer matrix, defined by the scattering potential $V(x)$ of the junction. In such a system, transfer-matrix formalism is more convenient than scattering-matrix formalism [47] due to the fact that we cannot neglect the effect of the magnetic field in the wires (as it determines the transition we study). For simplicity, we would proceed with the case of pointlike potential $V(x) = V_0 \delta(x)$, which gives [25]

$$T = 1 - i \frac{V_0}{\alpha} s_z + \frac{V_0}{\alpha} s_y, \quad (\text{A7})$$

where $s_{x,y,z}$ are the Pauli matrices acting in the space of left and right movers. We can introduce a transmission probability through the junction in the normal state [25]

$$D_N = \frac{1}{1 + (V_0/\alpha)^2}, \quad (\text{A8})$$

which is useful to write the boundary conditions:

$$\Psi_i(0^+) = \frac{e^{i\gamma \sigma_z}}{\sqrt{D_N}} [\Psi_i(0^-) + e^{-i\beta \sigma_z} \sqrt{1 - D_N} \Psi_o(0^-)], \quad (\text{A9})$$

$$\Psi_o(0^+) = \frac{e^{-i\gamma \sigma_z}}{\sqrt{D_N}} [\Psi_o(0^-) + e^{i\beta \sigma_z} \sqrt{1 - D_N} \Psi_i(0^-)]. \quad (\text{A10})$$

One can notice that these expressions contain two additional phases: γ is the forward-scattering phase in the normal state, β is the reflection phase in the normal state. However, performing a unitary transformation $\Psi_o \rightarrow e^{i\beta \sigma_z} \Psi_o$ the latter can be eliminated from equations, while for a delta function barrier the forward-scattering phase is given by [25]

$$\gamma = -\arctan \sqrt{\frac{1 - D_N}{D_N}}. \quad (\text{A11})$$

Now combining Eqs. (A4) and (A5) with the boundary conditions, one can write an equation determining the bound states

in the form [25]

$$\Lambda(E, \phi, D_N, V_Z) = 0, \quad (\text{A12})$$

where Λ is given by

$$\Lambda(E, \phi, D_N, V_Z) = \Lambda_0(E, \phi, V_Z) + (1 - D_N)\Lambda_1(E, \phi, V_Z) + (1 - D_N)^2\Lambda_2(E, \phi, V_Z) + D_N\Lambda_\gamma(E, \phi, V_Z)\sin^2\gamma; \quad (\text{A13})$$

$$\Lambda_0(E, \phi, V_Z) = \left[\Delta^2 \cos^2 \frac{\phi}{2} - E^2 \right] \left[\sqrt{\Delta_-^2 - E^2} \sqrt{\Delta_+^2 - E^2} \left(1 + \cos^2 \frac{\phi}{2} \right) - (E^2 + \Delta_- \Delta_+) \sin^2 \frac{\phi}{2} \right], \quad (\text{A14})$$

$$\begin{aligned} \Lambda_1(E, \phi, V_Z) = & \left[(E^2 + \Delta_- \Delta_+) \left(2\Delta^2 \cos^2 \frac{\phi}{2} - E^2 \right) - 2\Delta^2 E^2 \right] \sin^2 \frac{\phi}{2} \\ & + \sqrt{\Delta_-^2 - E^2} \sqrt{\Delta_+^2 - E^2} \left[\Delta \Delta_+ \cos^2 \frac{\phi}{2} - E^2 \right] + \sqrt{\Delta_-^2 - E^2} \sqrt{\Delta_+^2 - E^2} \left[\Delta \Delta_- \cos^2 \frac{\phi}{2} - E^2 \right] \\ & - \sqrt{\Delta_-^2 - E^2} \sqrt{\Delta_+^2 - E^2} \left[2\Delta^2 \cos^4 \frac{\phi}{2} - E^2 \left(1 + \cos^2 \frac{\phi}{2} \right) \right], \end{aligned} \quad (\text{A15})$$

$$\begin{aligned} \Lambda_2(E, \phi, B) = & \Delta^2 (E^2 + \Delta_- \Delta_+) \sin^4 \frac{\phi}{2} + \frac{1}{2} (\Delta_- \Delta_+ - E^2) [\Delta^2 \cos \phi - E^2] \\ & - \frac{1}{2} B^2 E^2 - \frac{1}{2} \sqrt{\Delta_-^2 - E^2} \sqrt{\Delta_+^2 - E^2} [\Delta \Delta_+ \cos \phi - E^2] - \frac{1}{2} \sqrt{\Delta_-^2 - E^2} \sqrt{\Delta_+^2 - E^2} [\Delta \Delta_- \cos \phi - E^2] \\ & + \frac{1}{2} \sqrt{\Delta_-^2 - E^2} \sqrt{\Delta_+^2 - E^2} \left[\Delta^2 \left(1 - \frac{1}{2} \sin^2 \phi \right) - E^2 \right], \end{aligned} \quad (\text{A16})$$

$$\Lambda_\gamma(E, \phi, V_Z) = \left[\Delta^2 \cos^2 \frac{\phi}{2} - E^2 \right] \left[-\sqrt{\Delta_-^2 - E^2} \sqrt{\Delta_+^2 - E^2} + \Delta_- \Delta_+ - E^2 \right]. \quad (\text{A17})$$

Here $\Delta_- = |\Delta - V_Z|$, the gap of the system, and $\Delta_+ = \Delta + V_Z$ are introduced for simplicity, γ is the forward scattering phase; for the toy model of a pointlike potential, it is given by Eq. (A11).

In this system, the continuum consisting of the scattering states above $|\Delta - V_Z|$ (or, more generally, the smallest gap in the system $\min[|\Delta - V_Z|, \Delta]$) should be taken into account, as it possesses a phase dependence (one can see it as a bound state merged into the continuum) and, therefore, affects the spectrum of the system already starting from the ground state, see Eq. (3). This phase-dependent contribution to the density of states in the continuum can be calculated via the same Λ expression [25]:

$$\delta\rho(E, \phi) = \frac{1}{2\pi i} \frac{\partial}{\partial E} \frac{\Lambda^*(E, \phi, D_N, V_Z)}{\Lambda(E, \phi, D_N, V_Z)}. \quad (\text{A18})$$

The spectrum in the high-transparency limit was analyzed in Refs. [25,41].

In this paper, we complement the analyses provided in previous works discussed above by studying the low-transparency limit, as it allows us to perform some estimations due to the simple cosine dependencies on the phase (tunneling regime). To begin, we expand

$$\sin^2\gamma = 1 - \frac{D_N}{4} + O(D_N^2). \quad (\text{A19})$$

Searching for the zeros of $\Lambda(E, \phi, D_N, V_Z)$ numerically, we see that the lowest ABS sticks to the gap, as expected, while the second ABS is completely merged with the continuum, see Fig. 4. The remaining ABS does not scale linearly with D_N , as in a trivial spin-degenerate ABS, but rapidly decays to zero with increase of V_Z . For each transmission amplitude

D_N , there is a value V_Z^{bs} , starting from which there is no bound state in the trivial phase, this value can be found as a solution of the equation:

$$\Lambda(\Delta - V_Z^{\text{bs}}, \pi, D_N, V_Z^{\text{bs}}) = 0. \quad (\text{A20})$$

From the numerical analysis, we can conclude that in the low-transparency case, the system has no bound states in a large vicinity of the phase transition, i.e., for $D_N = 0.3$ the bound state already disappears at $V_Z = 0.4328\Delta$. Therefore, we state that in a large vicinity of the transition, all the phase dependencies of the low-energy spectrum are determined by the phase-dependent density of states of the continuum, which allows us to state (in the main text) that there are no effects due to QP around the phase transition. Moreover, what is also interesting is that the total contribution (ABSs plus continuum) to the ground state in the trivial phase has a weak dependence on the magnetic field, which can be seen as if the continuum is acquiring a phase-dependent contribution from the ABSs merged into it. On the contrary, in the topological phase, the only bound-state amplitude scales as D_N at low transparency, as the continuum is gapped away from the bound state. We have calculated the amplitude in the low transparency limit expanding $\Lambda(E, \phi, D_N, V_Z)$ analytically in D_N and $E/(V_Z - \Delta)$ (see green and orange lines in Fig. 5),

$$E \approx 2 \frac{D_N \Delta}{V_Z} (V_Z - \Delta) \cos \frac{\phi}{2}, \quad (\text{A21})$$

which is Eq. (5) in the main text. What is a bit counterintuitive at first is the linear scaling with D_N , as naively it is expected to be the same as in Ref. [3] $\sim \sqrt{D_N}$, which corresponds to the single electron tunneling amplitude. The reason for this is that in Ref. [3] the edge states are supposed to carry only

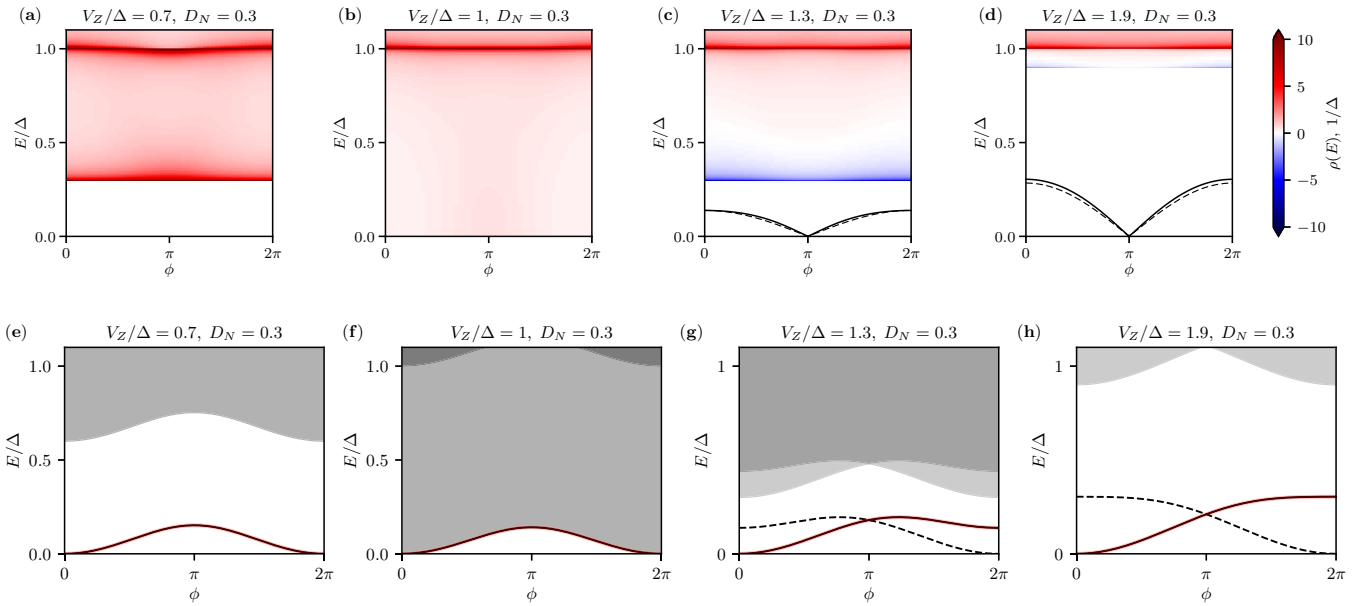


FIG. 4. Upper panels (a)–(d) show the single-particle spectrum at different values of Zeeman field V_Z as function of phase ϕ , corresponding to (a) trivial phase, (b) topological phase transition, and (c), (d) topological phase. The color over $|V_Z - \Delta|$ indicates the local density of states, while the black line below the gap corresponds to the bound state. (c), (d) In the topological phase, the dashed line corresponds to our analytical solution; we note that both parity solutions are depicted, one before π another one after π . (a) In the trivial phase, the bound state is absent for small $D_N = 0.3$. The lower panels (e)–(h) show the many-body spectrum of the junction versus ϕ at different values of V_Z ; the solid red line represents the ground state, the grey area is the continuum, and the dotted line represents an odd-parity state. (e) In the trivial state (at $V_Z/\Delta = 0.7$), the spectrum consists of the ground state and no discrete excited states up to the continuum (since there are no bound states); panel (f) shows the gapless spectrum at the phase transition; panel (g) corresponds to the topological phase at $V_Z/\Delta = 1.3$, each second local minimum of the ground state is suppressed by a 4π -periodic contribution, and panel (h) corresponds to the topological phase at $V_Z/\Delta = 1.9$, where only 4π -periodic local minima remain.

two helical modes, which is valid only at large Zeeman fields $V_Z \gg \Delta$ [25], where our formula is not applicable, as the SOI energy is no longer the largest energy scale in the system.

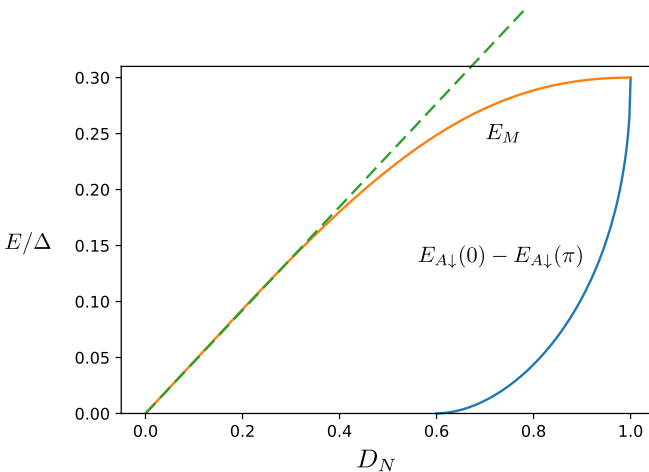


FIG. 5. Dependence of the bound-state amplitude on transmission amplitude D_N . The orange branch corresponds to the topological phase $V_Z = 1.3\Delta$, green dashed line is the analytical solution for low transparency given by Eq. (5); blue curve represents lowest ABS energy amplitude in the trivial phase for $V_Z = 0.7\Delta$ (difference of ABS energy at $\phi = 0$, when it touches the gap, and at $\phi = \pi$, when it is minimal). One can see that there is no ABS for low D_N , then starting from some value of transmission the bound state amplitude grows to the bulk gap size $\Delta_c = \Delta - V_Z$.

Now, we can write the many-body spectrum of the system. For the low-energy states, it is described by the occupation of bound states and continuum states below the superconducting gap Δ : From the numerical solution, we deduce that a parity switch close to the phase transition can only slightly modify the phase dependence of the system energy, as E_b is suppressed for small D_N or absent completely (all ABSs merging with continuum) and the main contribution to the low-energy spectrum comes from the scattering states in the continuum between the system gap $\Delta - V_Z$ and superconducting gap Δ . On the other side, deep inside the topological phase, a 4π -periodic bound state contribution dominates over the continuum contribution and, therefore, each parity switching event significantly changes the phase dependence of the system energy. The full picture of the spectrum evolution with Zeeman field can be seen in Fig. 4.

In a junction based on proximitized semiconducting nanowires with weak SOI, the Andreev limit is violated. Therefore, the regime is very hard to analyze analytically, however, we expect the qualitative behavior of the system to remain the same. At zero Zeeman field, two degenerate ABSs are present, the significant difference with strong SOI regime is the absence of zero-energy crossings at $\phi = \pi$ even for perfect transparency of the junction $D_N = 1$. In the presence of an external magnetic field, the ABSs split and get different amplitudes in the phase, as well as phase-dependent contributions from the continuum appear. Close to the topological phase transition, the continuum contribution to the ground state is dominating (on both sides of the transition). In the

topological phase, one would get 4π -periodic term due to hybridization of the two MBSs on the junction, however, the amplitude is determined not by the superconducting gap and Zeeman field $\Delta_c = V_Z - \Delta$, as in the strong SOI limit, but also by the SOI energy scale $E_{SO} = m\alpha^2/2$ [18,48]:

$$\Delta_c \approx 2\sqrt{\frac{E_{SO}}{V_Z}} \Delta. \quad (\text{A22})$$

Nevertheless, deep inside the topological phase, the MBS contribution is again dominating in the phase potential, therefore, the spectrum has the same features which are crucial for the observation of the effects discussed in the main text.

APPENDIX B: FINITE-SIZE EFFECTS IN THE TOPOLOGICAL PHASE

Here we analyze finite-size effects in the setup discussed in the main text and show that they do not significantly affect the proposed measurement. If there is a finite overlap with the MBSs on the outer edges of the topological part of the system, crossings at $\phi \approx (2k+1)\pi$ turn into anticrossings [45,46]. Strictly speaking, there are now four energy levels instead of two:

$$E_{\pm}^e = \pm \frac{1}{2} \sqrt{E_M^2 \cos^2 \frac{\phi}{2} + (\delta_L + \delta_R)^2}, \quad (\text{B1})$$

$$E_{\pm}^o = \pm \frac{1}{2} \sqrt{E_M^2 \cos^2 \frac{\phi}{2} + (\delta_L - \delta_R)^2}, \quad (\text{B2})$$

where the superscript e (o) stands for even (odd) parity solution, δ_L (δ_R) is the coupling with the MBS on the left (right) edge of the topological nanowire. What is important now is that the parity is the parity of the superposition of all four MBSs. Another issue worth mentioning is that δ_R and δ_L depend on the exact geometry of the nanowires forming the junction and can be both positive or negative. However, for each parity (which is fixed between parity switching events), the spectrum consist of two branches with fixed anticrossing $\delta = |\delta_L \pm \delta_R|$ (the sign of it being defined by the parity). If the phase evolution (relaxation) is fast enough in comparison to the splitting δ at the anticrossing, $\tau_{2\pi}^{-1} \gg \delta^2/(2E_M)$, a Landau-Zener transition (LZT) would let the system reach the lower branch and relax to a new 2π -shifted minimum as in the perfectly 4π -periodic case, see Fig. 6. However, if $R/R_Q \ll \delta^2/E_M^2$, which can be the case for strongly overdamped junctions and for finite δ , no LZT occurs and the state stays in the upper branch, thereby relaxing to the minimum at the anticrossing, giving rise to a voltage pulse of size $V = \frac{1}{2e} \frac{\pi}{\tau_\pi}$, where τ_π is the characteristic time for relaxation to a new π -shifted minimum. The next QP event will transfer the state to the lower branch with subsequent relaxation to a minimum, which also results in a π phase shift. Therefore, the average voltage will be twice smaller than in the 4π -periodic case [Eq. (6) in the main text]:

$$\langle V \rangle \approx \frac{1}{2e} \frac{\pi}{\tau_{qp}^{\text{top}}}. \quad (\text{B3})$$

If one can fine tune the overlap of the MBSs so in one parity state the splitting δ is large enough to suppress LZT and in another parity state it is very small (i.e., $\delta_L \approx \delta_R$ and

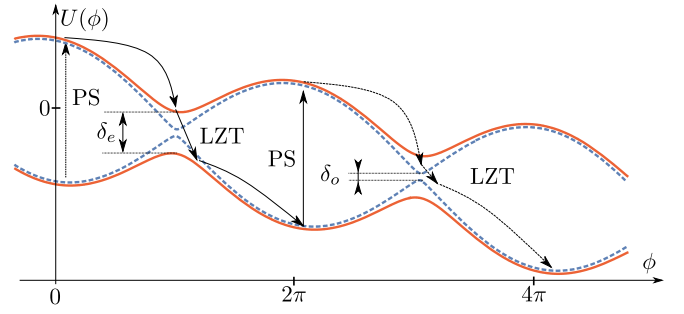


FIG. 6. The phase potential U for two different parities (solid red line for even parity and dashed blue for odd) as function of phase ϕ . Here we have chosen smaller splittings in the odd state than in the even state $\delta_o < \delta_e$, however, this does not need to be the case in general. Arrows correspond to phase evolution: vertical arrows marked with PS correspond to parity switches, arrows along the phase potential branches represent phase relaxation, LZT represents Landau-Zener transitions at the anticrossings. All solid arrows correspond to phase evolution in the even state (or starting in even state for phase switch), dashed arrows to that of the odd state.

$R/R_Q \ll 4\delta_L^2/E_M^2$), then it is possible to achieve an intermediate regime, where the average voltage is

$$\langle V \rangle \approx \frac{1}{2e} \frac{3\pi}{2\tau_{qp}^{\text{top}}}, \quad (\text{B4})$$

as after the parity switch the phase will relax by π or 2π depending on the parity.

APPENDIX C: VOLTAGE PULSES IN THE TRIVIAL PHASE

In this Appendix, we provide a detailed description of the QP effect in the trivial phase to supplement the discussion of the effect in the main text. If the junction is in the trivial phase, quasiparticles can be trapped in ABSs or recombine pairwise into the condensate of Cooper pairs. Both processes are rather slow (in comparison to getting trapped in the topological phase). Recombination is slow, since the recombination rate depends on the quasiparticle density quadratically ($\sim x_{qp}^2$, where $x_{qp} = n_{qp}/n_{Cp} \ll 1$ is the ratio of quasiparticle density and Cooper pair density), while the trapping rate to an ABS is low due to the small energy gap between the ABS energy and the continuum edge. If the bias current is zero, $I = 0$, the bound states touch the continuum edge at the phase values corresponding to the minima of the phase potential $\phi_{\min} = 2\pi k$ (k is integer), therefore, a quasiparticle cannot be trapped. For small bias current, $I \ll I_c$, the minima of the phase potential are slightly shifted, i.e., $\phi_{\min} \approx 2\pi k + \frac{1}{2eE_J}$, which results in a small energy gap between the continuum edge and the bound state $\epsilon = I^2/(4e^2E_J) \ll \Delta$ at ϕ_{\min} , which allows quasiparticle trapping in the bound states. As a result, at zero magnetic field, when a quasiparticle is trapped in an ABS, the only conducting channel will get poisoned, which would result in a running (resistive) state with voltage $V = IR$. Subsequently, the system will relax back to the ground state due to recombination of the trapped quasiparticle with a quasiparticle from the continuum on a timescale $\tau_r \ll \tau_{qp}^{\text{triv}}$. What is essential here is that the recombination rate of a quasiparticle trapped in the bound state with a quasiparticle from the continuum is linear

in the quasiparticle density $\sim x_{\text{qp}}$, as only one quasiparticle from the continuum is required. Therefore, the rate of such a recombination is sufficiently larger than the recombination rate for quasiparticle pairs from the continuum. At the same time, this recombination process releases the energy $\sim \Delta$ (in the form of a phonon), which makes it significantly more probable than the trapping of another quasiparticle from the continuum into the second ABS (releasing a phonon with much smaller energy $\epsilon \ll \Delta$), as normally at low energies the phonon density of states is increasing with energy (usually for metals it is quadratic $\nu_{\text{ph}} \sim E^2$). This can be seen from a simple estimate of the rate for a quasiparticle getting trapped into an ABS with energy E_A using a simplified model of a bulk superconductor [40],

$$\Gamma_t(\epsilon) = \pi x_{\text{qp}} \Delta \alpha_{e-\text{ph}}^2 \nu_{\text{ph}}(\Delta - E_A),$$

where $\alpha_{e-\text{ph}}$ is the electron-phonon interaction matrix element. For recombination processes, when one quasiparticle is trapped to an ABS and another one comes from the continuum edge, one can use the same formula for the recombination rate Γ_r , except replacing the phonon energy $\Delta - E_A = \epsilon$ by $\Delta + E_A \approx 2\Delta \gg \epsilon$. Under the assumption of a quadratic dependence of the phonon density of states on energy, one gets the ratio

$$\Gamma_r/\Gamma_t^{\text{triv}} \approx \frac{(2\Delta)^2}{\epsilon^2} \gg 1. \quad (\text{C1})$$

A similar formula can be used to estimate the ratio between quasiparticle trapping rates in the trivial and topological phases, which corresponds to Eq. (8) in the main text:

$$\begin{aligned} \Gamma_t^{\text{top}}/\Gamma_t^{\text{triv}} &\approx \frac{(\min[V_Z - \Delta, \Delta] - E_M)^2}{\epsilon^2} \\ &\approx \frac{(2e)^4 E_J^2 (1 - D_N)^2 \Delta^2}{I^4} \gg 1, \end{aligned} \quad (\text{C2})$$

since deep in the topological phase ($V_Z > 2\Delta$) the bound state is always separated from the continuum (except for the case of perfect transparency), while the energy gap between the ABS and the continuum in the trivial phase is small: $\epsilon \approx I^2/(4e^2 E_J) \ll \Delta$. We should note that QP rates in the topological phase, Γ_t^{top} , and relaxation rates in the trivial phase, Γ_r , (due to recombination of the trapped quasiparticle) can be of the same order, since the released phonons carry away energy of the order of the gap in both cases.

Turning on a magnetic field lowers the continuum edge ($\Delta - V_Z$) as well as splitting the ABSs. As a result, with one quasiparticle being trapped in one of the ABSs, the phase potential is no longer linear. According to numerical results provided in Refs. [25,41] for low fields a good approximation is to represent the energetically higher ABS plus continuum just as an effective higher ABS (which is merged in the continuum between $\Delta - B$ and Δ). Then, we can represent the lower ABS energy as $E_{A2} = (\Delta - V_Z) - E_{J2}(1 - \cos \phi)$, while the combination of a higher ABS and continuum contribution is given by $E_{A1} = \Delta - E_{J1}(1 - \cos \phi)$. Moreover, in the Andreev limit we can express the amplitudes through the transmission coefficient D_N (as, in general, $E_A = \Delta \sqrt{1 - D_N \sin^2 \frac{\phi}{2}} \approx \Delta - \frac{\Delta D_N}{4}(1 - \cos \phi)$). Then, $E_{J2} \approx D_N(\Delta - V_Z)/4$, $E_{J1} \approx D_N \Delta/4$. As a result, we

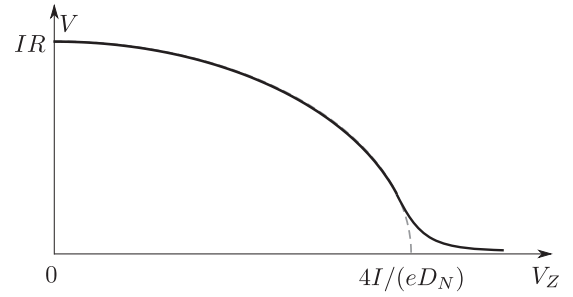


FIG. 7. A schematic of the average voltage dependence on the applied magnetic field (Zeeman field V_Z) in the running state (excitation due to absorption of one quasiparticle). The blue dashed line is given by Eq. (4). The deviation from the dashed line is caused by thermal fluctuations, such as thermally activated phase slips, when the local minima of the phase potential are shallow.

can use $E_{J1} - E_{J2} \approx D_N V_Z/4$ for the low-transparency limit (in the high-transparency limit it is given by $E_{A1}(\pi) - E_{A2}(\pi) \approx V_Z$, which is also linear in V_Z). Then, in leading order the difference between the amplitudes of the ABSs is determined by the Zeeman term V_Z . The effective phase potential takes the form:

$$U(\phi) = -\frac{1}{2}(E_{J1} + (-1)^n E_{J2}) \cos \phi - \frac{I\phi}{2e}, \quad (\text{C3})$$

which corresponds to Eq. (2) of the main text with the 4π -periodic term set to zero (no MBSs). Here $n = 0, 1$ denotes the occupation of the energetically lower lying ABS; we assume the occupation of the higher ABS to be constant (it sticks to the continuum edge in some vicinity of $\phi = 2\pi k$). Then, for $n = 0$, the potential has deep enough local minima to keep the phase localized, as we assume small currents $I \ll e(E_{J1} + E_{J2}) \approx eD_N \Delta/2$. However, the first excited state $n = 1$ may not have local minima, depending on the ratio $I/(eV_Z D_N)$. At low fields, the system is in the running state (no local minima). The effective critical current depends on the amplitude of the phase potential: $I_c = e(E_{J1} - E_{J2}) \approx eD_N V_Z/4$. For the running state in the RSJ model, the phase evolution is given by the classical equation of motion:

$$\frac{d\phi}{dt} = 2eI_c R \left(\frac{I}{I_c} - \sin \phi \right). \quad (\text{C4})$$

The known solution for the average voltage in the running state is [24]

$$\begin{aligned} \langle V \rangle &= R \sqrt{I^2 - I_c^2} = R \sqrt{I^2 - e^2 V_Z^2 D_N^2 / 16} \\ &\approx IR - \frac{e^2 D_N^2 V_Z^2}{32I} R, \end{aligned} \quad (\text{C5})$$

which corresponds to Eq. (4); the last approximation is an expansion in small magnetic field. One should note that now it is the average voltage in the running state, as it is varying in time, which can be easily seen from a simple model of a particle sliding down a one-dimensional washboard potential (without local minima) with friction. The higher the field, the longer the system spends in the lower voltage regime (i.e., the flatter parts of the washboard potential) with short intervals

of voltages exceeding the average value (steeper parts of the phase potential). Moreover, we expect a smearing around $V_Z = 4I/(eD_N)$, where the voltage goes to zero according to the formula Eq. (C5) (without expansion in small magnetic field) due to thermal fluctuations (thermally activated phase slips for shallow local minima of the phase potential), see Fig 7.

As a result, in the trivial state with low magnetic fields, QP would result in rare switching to the running state with an average voltage given by Eq. (C5) and lasting for a short time $\tau_r = 1/\Gamma_r \ll \tau_{qp}^{\text{triv}}$, where $\tau_{qp}^{\text{triv}} = 1/\Gamma_t$ is the characteristic time between QP events (quasiparticles getting trapped in the lower ABS). However, for larger magnetic fields, $V_Z \gtrsim 4I/(eD_N)$, no voltage will develop in the trivial phase.

-
- [1] A. Y. Kitaev, *Phys. Usp.* **44**, 131 (2001).
- [2] H.-J. Kwon, K. Sengupta, and V. M. Yakovenko, *Eur. Phys. J. B* **37**, 349 (2003).
- [3] L. Fu and C. L. Kane, *Phys. Rev. B* **79**, 161408(R) (2009).
- [4] J. Wiedenmann, E. Bocquillon, R. Deacon, S. Hartinger, O. Herrmann, T. M. Klapwijk, L. Maier, C. Ames, C. Brüne, C. Gould, A. Oiwa, K. Ishibashi, S. Tarucha, H. Buhmann, and L. W. Molenkamp, *Nat. Commun.* **7**, 10303 (2016).
- [5] P. J. de Visser, J. J. A. Baselmans, P. Diener, S. J. C. Yates, A. Endo, and T. M. Klapwijk, *Phys. Rev. Lett.* **106**, 167004 (2011).
- [6] G. Goldstein and C. Chamon, *Phys. Rev. B* **84**, 205109 (2011).
- [7] D. Rainis and D. Loss, *Phys. Rev. B* **85**, 174533 (2012).
- [8] J. C. Budich, S. Walter, and B. Trauzettel, *Phys. Rev. B* **85**, 121405(R) (2012).
- [9] T. Karzig, C. Knapp, R. M. Lutchyn, P. Bonderson, M. B. Hastings, C. Nayak, J. Alicea, K. Flensberg, S. Plugge, Y. Oreg, C. M. Marcus, and M. H. Freedman, *Phys. Rev. B* **95**, 235305 (2017).
- [10] C. Knapp, T. Karzig, R. M. Lutchyn, and C. Nayak, *Phys. Rev. B* **97**, 125404 (2018).
- [11] T. Karzig, W. S. Cole, and D. I. Pikulin, *Phys. Rev. Lett.* **126**, 057702 (2021).
- [12] L. Fu and C. L. Kane, *Phys. Rev. Lett.* **100**, 096407 (2008).
- [13] Y. Oreg, G. Refael, and F. von Oppen, *Phys. Rev. Lett.* **105**, 177002 (2010).
- [14] A. M. Black-Schaffer and J. Linder, *Phys. Rev. B* **83**, 220511(R) (2011).
- [15] A. Murani, A. Kasumov, S. Sengupta, Y. A. Kasumov, V. T. Volkov, I. I. Khodos, F. Brisset, R. Delagrè, A. Chepelianskii, R. Deblock, H. Bouchiat, and S. Guéron, *Nat. Commun.* **8**, 15941 (2017).
- [16] Y. Bernard, A. Peng, A. Kasumov, R. Deblock, M. Ferrier, F. Fortuna, V. T. Volkov, Y. A. Kasumov, Y. Oreg, F. von Oppen, H. Bouchiat, and S. Guéron, [arXiv:2110.13539](https://arxiv.org/abs/2110.13539).
- [17] Y. Tanaka, T. Yokoyama, and N. Nagaosa, *Phys. Rev. Lett.* **103**, 107002 (2009).
- [18] J. Klinovaja and D. Loss, *Phys. Rev. B* **86**, 085408 (2012).
- [19] H.-J. Kwon, K. Sengupta, and V. M. Yakovenko, *Low Temp. Phys.* **30**, 613 (2004).
- [20] S.-P. Lee, K. Michaeli, J. Alicea, and A. Yacoby, *Phys. Rev. Lett.* **113**, 197001 (2014).
- [21] D. Frombach and P. Recher, *Phys. Rev. B* **101**, 115304 (2020).
- [22] R. M. Lutchyn, J. D. Sau, and S. Das Sarma, *Phys. Rev. Lett.* **105**, 077001 (2010).
- [23] K. K. Likharev and A. B. Zorin, *J. Low Temp. Phys.* **59**, 347 (1985).
- [24] M. Tinkham, in *Introduction to Superconductivity*, 2nd ed. (McGraw-Hill Book Co., New York, 1996).
- [25] C. Murthy, V. D. Kurilovich, P. D. Kurilovich, B. van Heck, L. I. Glazman, and C. Nayak, *Phys. Rev. B* **101**, 224501 (2020).
- [26] S. Diamond, V. Fatemi, M. Hays, H. Nho, P. D. Kurilovich, T. Connolly, V. R. Joshi, K. Serniak, L. Frunzio, L. I. Glazman, and M. H. Devoret, [arXiv:2204.07458](https://arxiv.org/abs/2204.07458) (2022).
- [27] J. M. Martinis, M. Ansmann, and J. Aumentado, *Phys. Rev. Lett.* **103**, 097002 (2009).
- [28] K. Segall, C. Wilson, L. Li, L. Frunzio, S. Friedrich, M. C. Gaidis, and D. E. Prober, *Phys. Rev. B* **70**, 214520 (2004).
- [29] S. B. Kaplan, C. C. Chi, D. N. Langenberg, J. J. Chang, S. Jafarey, and D. J. Scalapino, *Phys. Rev. B* **14**, 4854 (1976).
- [30] J. Aumentado, M. W. Keller, J. M. Martinis, and M. H. Devoret, *Phys. Rev. Lett.* **92**, 066802 (2004).
- [31] J. A. Schreier, A. A. Houck, J. Koch, D. I. Schuster, B. R. Johnson, J. M. Chow, J. M. Gambetta, J. Majer, L. Frunzio, M. H. Devoret, S. M. Girvin, and R. J. Schoelkopf, *Phys. Rev. B* **77**, 180502(R) (2008).
- [32] M. D. Shaw, R. M. Lutchyn, P. Delsing, and P. M. Echternach, *Phys. Rev. B* **78**, 024503 (2008).
- [33] L. Sun, L. DiCarlo, M. D. Reed, G. Catelani, L. S. Bishop, D. I. Schuster, B. R. Johnson, G. A. Yang, L. Frunzio, L. Glazman, M. H. Devoret, and R. J. Schoelkopf, *Phys. Rev. Lett.* **108**, 230509 (2012).
- [34] L. Cardani, F. Valenti, N. Casali, G. Catelani, T. Charpentier, M. Clemenza, I. Colantoni, A. Cruciani, G. D’Imperio, L. Gironi, L. Grünhaupt, D. Gusenkova, F. Henriques, M. Lagoin, M. Martinez, G. Pettinari, C. Rusconi, O. Sander, C. Tomei, A. V. Ustinov, M. Weber, W. Wernsdorfer, M. Vignati, P. S., and I. M. Pop, *Nat. Commun.* **12**, 2733 (2021).
- [35] J. M. Martinis, *npj Quantum Inf.* **7**, 90 (2021).
- [36] G. Catelani and J. P. Pekola, *Mater. Quantum. Technol.* **2**, 013001 (2022).
- [37] A. P. Vepsäläinen, A. H. Karamlou, J. L. Orrell, A. S. Dogra, B. Loer, F. Vasconcelos, D. K. Kim, A. J. Melville, B. M. Niedzielski, J. L. Yoder, S. Gustavsson, J. A. Formaggio, B. A. VanDevender, and W. D. Oliver, *Nature (London)* **584**, 551 (2020).
- [38] A. Bespalov, M. Houzet, J. S. Meyer, and Y. V. Nazarov, *Phys. Rev. Lett.* **117**, 117002 (2016).
- [39] O.-P. Saira, A. Kemppinen, V. F. Maisi, and J. P. Pekola, *Phys. Rev. B* **85**, 012504 (2012).
- [40] E. M. Levenson-Falk, F. Kos, R. Vijay, L. Glazman, and I. Siddiqi, *Phys. Rev. Lett.* **112**, 047002 (2014).
- [41] P. San-Jose, J. Cayao, E. Prada, and R. Aguado, *New J. Phys.* **15**, 075019 (2013).

- [42] E. Prada, P. San-Jose, M. W. A. de Moor, A. Geresdi, E. J. H. Lee, J. Klinovaja, D. Loss, J. Nygård, R. Aguado, and L. P. Kouwenhoven, *Nat. Rev. Phys.* **2**, 575 (2020).
- [43] C. W. J. Beenakker, D. I. Pikulin, T. Hyart, H. Schomerus, and J. P. Dahlhaus, *Phys. Rev. Lett.* **110**, 017003 (2013).
- [44] P. P. Aseev, P. Marra, P. Stano, J. Klinovaja, and D. Loss, *Phys. Rev. B* **99**, 205435 (2019).
- [45] F. Domínguez, F. Hassler, and G. Platero, *Phys. Rev. B* **86**, 140503(R) (2012).
- [46] D. I. Pikulin and Y. V. Nazarov, *Phys. Rev. B* **86**, 140504(R) (2012).
- [47] B. van Heck, J. I. Väyrynen, and L. I. Glazman, *Phys. Rev. B* **96**, 075404 (2017).
- [48] J. Cayao, P. San-Jose, A. M. Black-Schaffer, R. Aguado, and E. Prada, *Phys. Rev. B* **96**, 205425 (2017).